Investigating the FSW parameter's role on microstructure and mechanical properties of welding AZ31B–AA8110 alloy

S. DHARMALINGAM[1]*, K. LENIN[2], and D. SRINIVASAN[2]

[1] Department of Mechanical Engineering, OASYS Institute of Technology, Trichy, Tamil Nadu, India
[2] Department of Mechanical Engineering, K. Ramakrishnan College of Engineering, Trichy, Tamil Nadu, India

Abstract. The influence of friction stir welding (FSW) in automotive applications is significantly high in recent days as it can boast beneficial factors such as less distortion, minimized residual stresses and enhanced mechanical properties. Since there is no emission of harmful gases, it is regarded as a green technology, which has an energy efficient clean environmental solid-state welding process. In this research work, the FSW technique is employed to weld the AA8011–AZ31B alloy. In addition, the L16 orthogonal array is employed to conduct the experiments. The influences of parameters on the factors such as microstructure, hardness and tensile strength are determined. Microstructure images have shown tunnel formation at low rotational speed and vortex occurrence at high rotational speed. To attain high quality welding, the process parameters are optimized by using a hybrid method called an artificial neural network based genetic algorithm (ANN-GA). The confirmation tests are carried out under optimal welding conditions. The results obtained are highly reliable, which exhibits the optimal features of the hybrid method.

Key words: AA8011–AZ31B alloy; FSW; ANN-GA; mechanical properties.

1. INTRODUCTION

The industries are still searching for light-weight dissimilar welded alloys for automotive applications [1] to save the energy and manufacturing components with optimized material properties. Magnesium (Mg) alloys are light-weight structural materials, which have a hexagonal closed pack structure with 1.74 g/m^3 density [2]. Aluminum (Al) alloys have face-centered cubic structure with a density of 2.84 g/m^3. Because of having the distinct crystal structure, it is not easy to weld both Mg and Al alloys by means of conventional welding techniques [3]. Hence, the advanced joining technique of friction stir welding (FSW) is highly preferable in achieving better mechanical properties with defect-free welding [4,5]. Various studies have been conducted to investigate the importance of materials, welding parameters and tool design [6–13]. The significance of friction pressure on the microstructure has also been investigated [14]. Increased friction pressure improves tensile strength. The role of pin adhesion for joint quality of welding a 6061 T6Al / AZ31B Mg alloy at 60 mm/min welding speed is showed, which has eliminated the adhesion phenomenon, allowing to attained higher tensile properties [15]. To enhance welding quality, it is necessary to find the optimal FSW parameters [16,17].

For attaining parameter optimization, certain advanced optimization tools like ANN, adaptive neuro fuzzy interface system (ANFIS), particle swarm optimization (PSO), response surface methodology (RSM) and genetic algorithm (GA) have been used by many researchers [18,19]. Hamed *et al.* [20] have applied ANN-GA to attain an optimal parameter solution for welding the AA 5502 as AISI 304, in which the confirmation test is carried out to show the improvement in tensile strength and elongation. Zhen *et al.* [21] have used the back propagation neural network (BPNN)-GA for the optimized input parameters of laser brazing in the crimping butt, which enhances the stability and efficacy of the process. The cryo-rolled AA2219 alloy has been welded by means of FSW, in which the ANN-GA is employed for optimizing the welding parameters such as the tool tilt angle, travel speed and rotational speed [22]. Edwin *et al.* [23] have proposed the ANN-GA for optimizing the parameter of the diffusion bonding process to improve the tensile and shear strength of both the AA6061 and AA7075 joints. Hongyang *et al.* [24] have employed the hybrid laser TIG welding process to join the carbon fiber reinforced polymer and an Al alloy. In addition, the BPNN-GA has been utilized to assess the optimum process variables with the accuracy of 97%.

Moreover, researchers have conducted various studies on the welding processes of dissimilar Al alloys using FSW. However, no literature entries have reported the optimization of parameters in the welding process of the AZ31B–AA8011 alloy. The optimization of process parameters is vital for attaining a high-quality weld. To understand the impact of process parameters on the microstructure and mechanical properties such as micro-hardness & tensile strength, the necessity of process parameter optimization is extremely essential.

*e-mail: sdarmalingam79@gmail.com

Bull. Pol. Acad. Sci. Tech. Sci., vol. 70, no. 1, p. e140098, 2022

1

In the present research work, the hybrid ANN-GA is applied to upgrade the FSW process parameters for maximizing tensile strength and microhardness. The validation test is carried out to predict the accuracy. In addition, the metallurgical investigation is performed under the optimal welding conditions.

2. EXPERIMENTAL STUDY

The AZ31B Mg alloy and AA8011 Al alloy are the commonly utilized base plates of FSW. In this study, 32 pieces are taken with the size of 50 mm × 50 mm × 3.5 mm for the welding process. The chemical compositions of the base plates are listed in Table 1.

Table 1
Chemical composition of grade AZ31B and AA8011

% (Wt.)	Cu	Si	Mn	Mg	Ti	Cr	Fe	Zn	Al
Grade AZ31B	–	0.02	0.294	96.19	–	–	–	0.75	2.74
Grade AA8011	0.015	0.62	0.11	0.02	0.001	0.03	0.8	0.04	98.364

The flattened edges of the base plates are thoroughly cleaned before the welding process [25]. The square butt joint is employed for the welding process. Parameters such as rotational speed in rpm, tool type and welding speed in mm per minute are selected with four levels for the welding process, which is shown in Table 2. The literature review explains the influence of these three parameters, which play a prominent role in the welding performance. In the welding process, the AA8011 Al base plate is kept in the advancing side (AS) and the AZ31B Mg base plate is kept in the retreating side (RS). Four different-shape tools like taper with threaded pin (TH), taper cylindrical pin (TC), square pin (SQ) and triangle pin (TR) are used in the welding process [26].

Table 2
Levels and input parameters

S. No.	Parameters/Levels	I	II	III	IV
1	Tool type	TH	TC	SQ	TR
2	Rotational speed (RPM)	500	1000	1500	2000
3	Welding speed (mm/Min)	20	25	30	35

When considering the number of parameters and levels, the L16 orthogonal array is employed to complete the welding process. The performance of each welded joint is measured through microstructure, Vickers microhardness and tensile test. As per the ASM handbook, the samples of optical microscope are prepared and examined by the Universal Metallography Versamet and Clemex image analyzing system. In accordance with ASTM E384, the Vickers microhardness test is performed on a 500g load for 10s dwell time in the Zwick microhardness testing instrument. The ASTM E8M standard is followed for the preparation and testing of tensile test sample. The tensile

test is conducted in a FIE servo-controlled universal testing machine. Figure 1(a) shows the 32 welded experimental samples and Fig. 1(b) shows the fractured tensile samples.

Fig. 1. (a) Welded specimens, (b) tensile specimens after fracture

3. ANN-GA MODEL

The ANN [27, 28] involves training and testing processes, in which 80% of actual data are employed for training and 20% of the actual data are used for testing. The feed forward back propagation (FFBP) neural network [29] is preferred for this study, which is developed by MATLAB 7.1. The structure consists of three input parameters and two output responses (Vickers microhardness and tensile strength). The structure of ANN with two hidden layers is demonstrated in Fig. 2.
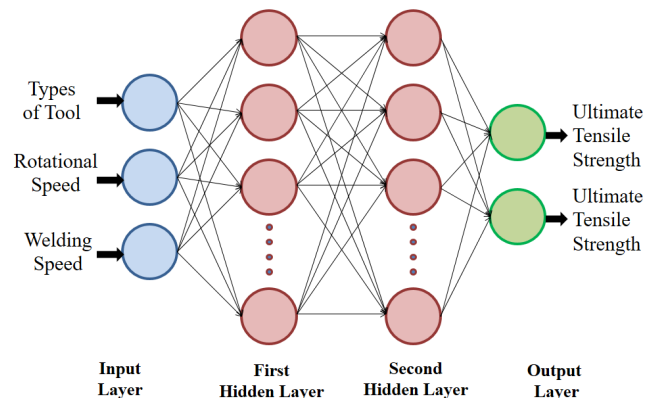

Fig. 2. ANN architecture

GA is the best optimization tool, which consists of five steps including population, fitness function, reproduction, crossover and mutation. The algorithm regenerates the population of individual solutions until an optimal solution set is obtained. GA has used the crossover and mutation operations to generate new chromosomes with better fitness. By the process of crossover, the parents are formed and the feasible solution called offspring is created. In each iteration, GA has selected the solution sets from the population through the randomizing technique to produce offspring for the next iteration. Random modifications are carried out in the chromosomes by the mutation process [30].

The integrated GA and ANN algorithm is implemented for maximizing microhardness and ultimate tensile strength. The process of hybrid GA -based ANN is illustrated in a flow diagram as shown in Fig. 3.
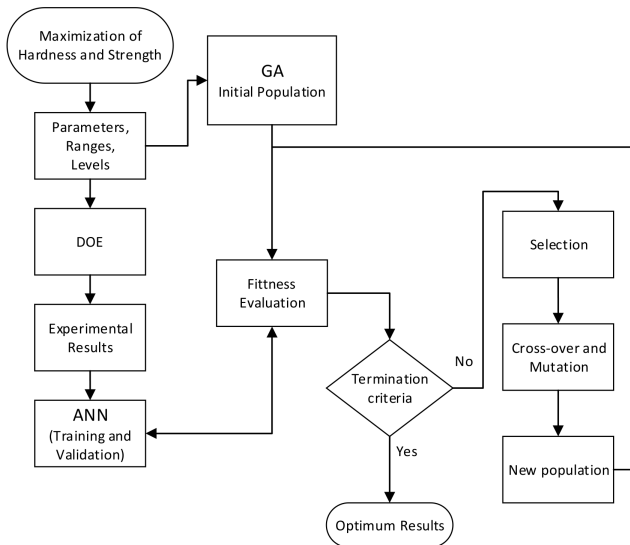
2

Bull. Pol. Acad. Sci. Tech. Sci., vol. 70, no. 1, p. e140098, 2022

Fig. 3. Flow chart of hybrid GA and ANN model

4. RESULTS AND DISCUSSION

The experimental outputs of the test are presented in Table 3. The role of FSW process parameters in the microstructure and mechanical properties are elaborated in this section.

Table 3
Experimental result of AA8011–AZ31 B

S. No.	Tool type	Rotational speed (rpm)	Welding speed (mm/min)	Ultimate tensile strength (MPa)	Micro-hardness (Hv)
1	TH	500	20	115	77.95
2	TH	1000	25	124	82.6
3	TH	1500	30	129	77.95
4	TH	2000	35	131	81.4
5	TC	500	25	118	76.95
6	TC	1000	20	138	76.15
7	TC	1500	35	132	80.85
8	TC	2000	30	124	84.05
9	SQ	500	30	103	81.1
10	SQ	1000	35	124	72.75
11	SQ	1500	20	115	69.6
12	SQ	2000	25	121	60.85
13	TR	500	35	117	73.9
14	TR	1000	30	130	75.5
15	TR	1500	25	125	81.2
16	TR	2000	20	112	76.6

4.1. Microstructure

Figure 4 shows the optical microstructure of a stir zone under different parameter conditions. The TH tool rotation at 500 rpm has resulted in tunnel formation on one side of the stir zone,

which is exhibited in Fig. 4(a). This is caused possibly by the insufficient heat generation of material flow. Similar observations have already been made in the literature [15, 31, 32].
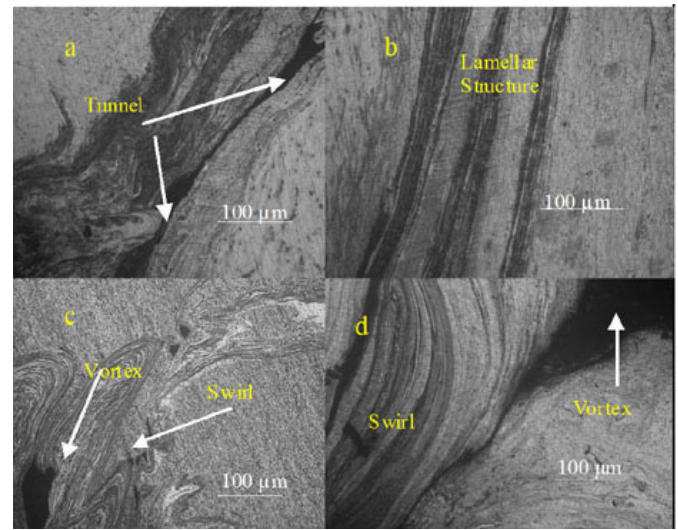

Fig. 4. Optical microstructure of FSW stir zone for different parameter conditions as: (a) TH, 500 rpm, 20 mm/min, (b) TC, 1000 rpm, 20 mm/min, (c) SQ, 2000 rpm, 25 mm/min, (d) TR, 2000 rpm, 20 mm/min

The lamellar structure occurred at 1000 rpm of the TC tool, in which the new crystal grains are created in the lamellar grains by the generation of high thermal energy. The same occurrence is reported in the work of Liangliang *et al.* [33]. The increasing rotational speed and tool type are the reason for the lamellar structure formation, which is depicted in Fig. 4(b). At 2000 rpm with 20 mm/min, the SQ tool forms a swirl and vortex in the stir zone (SZ), as highlighted in Fig. 4(c). The swirl mixture is formed by the turbulent flow of the material under the tool pin [34]. The occurrence of a swirl and vortex on the TR tool at 2000 rpm and 20 mm/min is exhibited in Fig. 4(d).

4.2. Mechanical properties

Based on the type of tool used, the variation of rotational speed has fluctuated along the tensile strength, as depicted in Fig. 5. Due to the poor diffusion of the joints, the tool rotational speed at 500 rpm shows low tensile strength and welding speed without considering the tool types. Rotational speed is increased up to 1500 rpm, which rapidly improves tensile strength of all the specimens. However, the specimen with the SQ tool has further raised the rotational speed into 2000 rpm, which has suddenly reduced the tensile strength for all the specimens. This is actually caused by the higher heat dissipation, which results in poor bonding.

Figure 6 presents the influence of welding speed on tensile strength. The minimum speed of 20mm/min has exhibited low tensile strength for specimens with TH, SQ and TR tools. Irrespective of tool type and rotational speed, tensile strength consequently improved for other welding speeds. The TC tool specimen with 35 mm/min welding speed and 1500 rpm rotational speed shows better strength than other combinations.
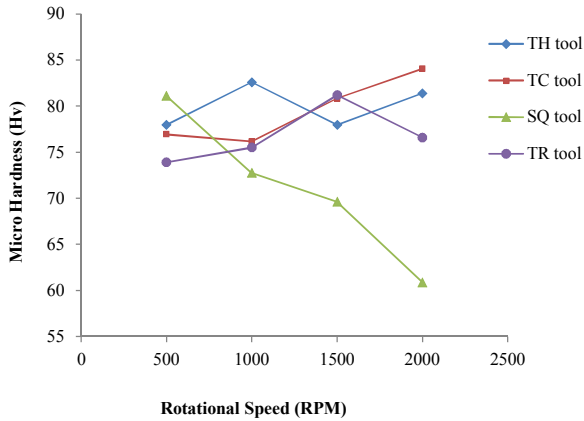
Bull. Pol. Acad. Sci. Tech. Sci., vol. 70, no. 1, p. e140098, 2022

3

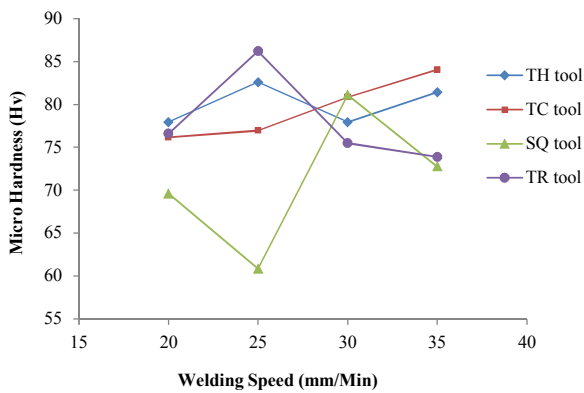**Fig. 5.** Rotational speed vs. tensile strength

Fig. 6. Welding speed vs. tensile strength

This feasible parameter condition has significantly reduced the heat affected zone in the joints, through which tensile strength is enhanced.

The microhardness value for different rotation speeds is portrayed in Fig. 7. The increase in the rotational speed has reduced the microhardness value for the specimen with the SQ tool. For the specimen with the TC tool, higher microhardness of 84.05 Hv is achieved at 2000 rpm. Figure 8 shows the microhardness of different tools with varying welding speed. The TR tool at 25 mm/min welding speed has produced the highest microhardness value.
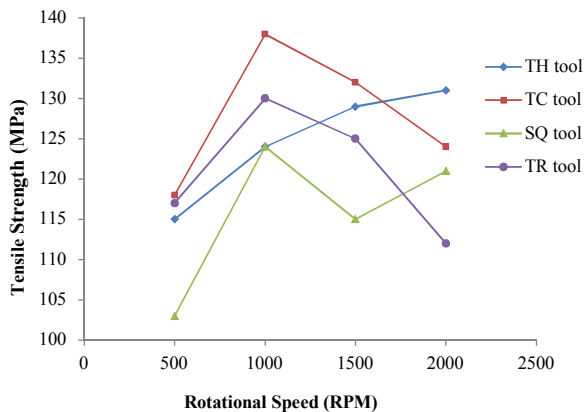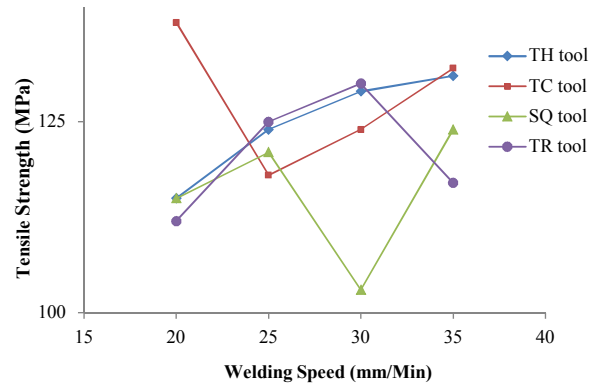

Fig. 7. Microhardness vs. rotational speed

Fig. 8. Microhardness vs. welding speed

4.3. Optimization of FSW parameters

The feed forward back propagation (FFBP) neural network is adopted to train the ANN. In FFBP, the input parameters are applied to the input layer, which are then propagated into the output layer through the hidden layer by using a transfer function with the initial weights. With the error between the target value and the output in mind, the weights are adjusted from the output to input layer, which is termed back propagation. The training performance of the ANN is illustrated in Fig. 9. It is trained by using the results, which are presented in Table 3. The implemented parameters of ANN training are shown in Table 4. Consequently, the trained network is tested with new sets of experimental results and the prediction error is found to be less than 1%. The fitness value of objective function is found by using the trained ANN. In GA, the elitism concept has been adopted to retain some of the best chromosomes for the next generation. In the present study, the elite count is 0.05 times higher than the initial population size. The mutation factor is selected as 1%. The scattered crossover is employed to perform the crossover operation since the chromosomes are coded with real values. The termination criterion of the GA process is set either as the convergence of the results with the same values or as 1500 iterations.
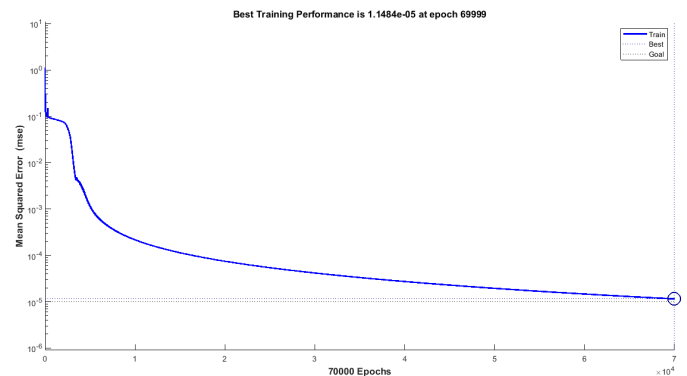

Fig. 9. ANN training performance

Figure 10 represents the graph which is plotted between the objective function and iteration. Optimized parameters such as the taper cylindrical pin tool type, 1653 rpm rotational speed and 20 mm/min welding speed are obtained, and they produce

4

Bull. Pol. Acad. Sci. Tech. Sci., vol. 70, no. 1, p. e140098, 2022

Table 4
Experimental result of AA8011–AZ31 B

S. No.	Parameters used in ANN training	Values
1	Network configuration	3-10-10-1
2	No. of neurons in input layer	3
3	No. of neurons in output layer	1
3	Maximum no. of epochs	70000
4	Goal (mean square error)	0.00001
5	Activation functions for hidden and output layers	Tansig
6	Activation function for input layer	Logsig
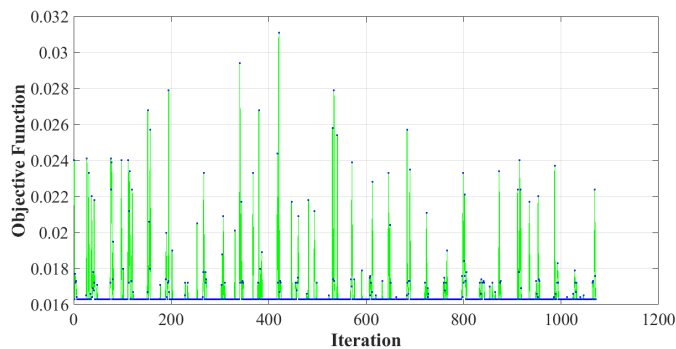
**Fig. 10.** Objective functions vs. iteration plot

the ultimate tensile strength of 139.46 MPa and hardness of 85.97 Hv with the total run of 1070 iterations.

5. CONFIRMATION TEST

The confirmation test has been performed under the optimal condition, which is obtained by the ANN-GA technique. In the optimal condition, the AA8011–AZ31B alloys are welded and the performances of these alloys are investigated through techniques such as microstructure analysis, microhardness and tensile strength testing.
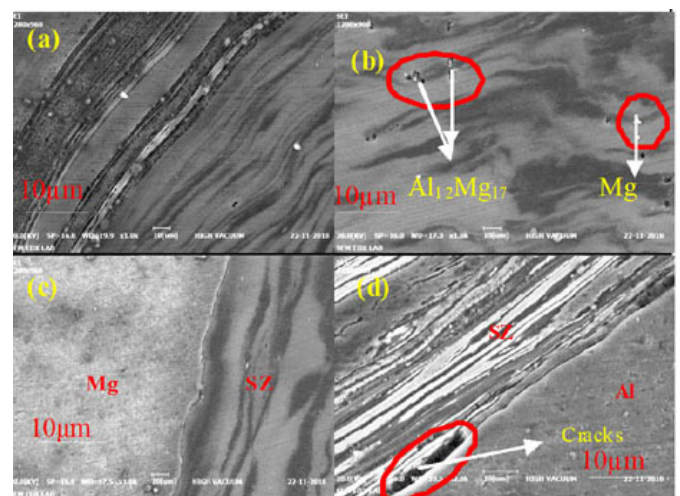
5.1. Microstructure

Figures 11(a) and 11(b) represents the microstructure of SZ under optimal parameter conditions. Al/Mg are strongly interlocked and no cracks are seen in the joints. The mechanical components of the Al/Mg joint have depended on the interlocking of joints, which are seen through the microstructure [15].
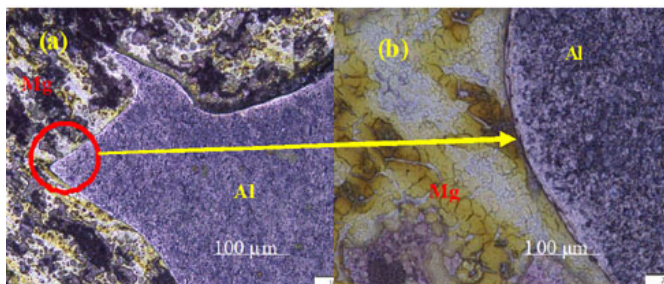
**Fig. 11.** Optical microstructure of FSW-SZ under optimal condition (a), (b) magnification of (a)

The optimal parameter conditions and proper placing of work piece have improved the formation of an intercalated layer in the SZ. It has enhanced the mechanical interlocking and formation of an intermetallic compound, which results in the increment of bonding strength [35].

Figure 12(a–d) illustrates the SEM microstructure of the FSW stir zone under the optimal condition. The intercalated layer is observed in the SZ, as illustrated in Fig. 12(a). However, more intercalated layers are developed towards the edges of the Al/Mg face, which supports mechanical interlocking. A similar observation has been reported in the literature [36]. The intermetallic compound ($Al_{17}Mg_{12}$) is formed in the SZ, as represented in Fig. 12(b). Through Figs. 12(c) and 12(d), it is noted that there is no crack formation on the edges of AS and RS.

Fig. 12. SEM microstructure of FSW stir zone under optimal condition (a) and (b) SZ, (c) SZ edge of RS, (d) SZ edge of AS

5.2. XRD

Figure 13 depicts the XRD spectrum of SZ under the optimal condition. The results have revealed the formation of an intermetallic compound ($Al12Mg17$) in the SZ. This newly developed compound has increased the strength of the joints. Similar observations have been reported in [32, 37, 38].
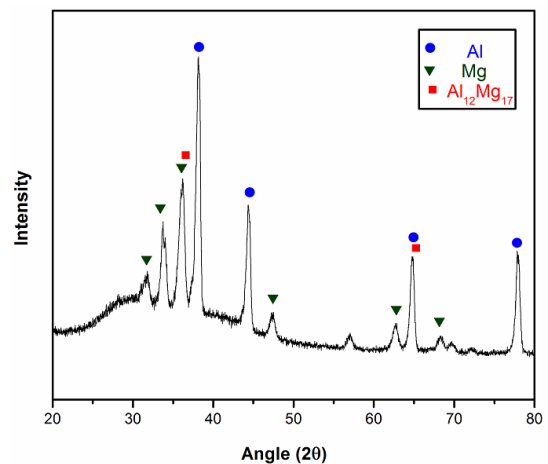
Fig. 13. XRD of SZ under optimal condition

Bull. Pol. Acad. Sci. Tech. Sci., vol. 70, no. 1, p. e140098, 2022

5

5.3. Micro hardness

At the top surface of the welded plate, microhardness is measured for each 5 mm interval from the center point of SZ on either side. Figure 14 depicts the values, which fluctuate on both sides. This uneven distribution occurs due to the presence of the intermetallic compound in the SZ. Moreover, hardness is increased by the stirring effect in SZ, which refines the grain size [36]. Microhardness decreases towards the edges of AS and RS, away from the center point of SZ. Maximum hardness of 80.13 Hv is attained at the center point. The heat affected zone (HAZ) of RS delivers low hardness of 57.72 Hv.
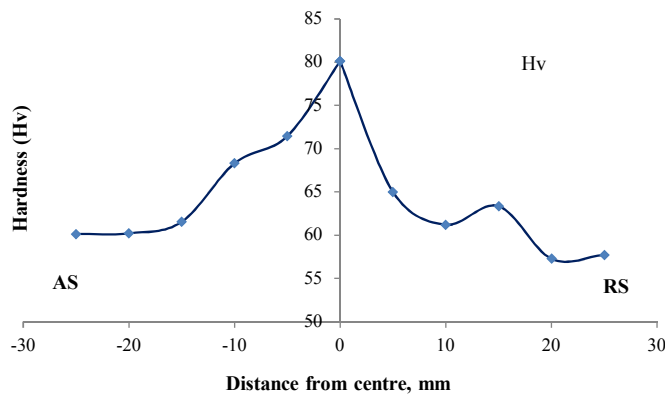

Fig. 14. Microhardness distribution of Al/Mg joint at top side

5.4. Tensile strength

Figure 15 presents tensile strength of the joint under the optimal parameter condition. Tensile strength has reached 138 MPa, which is almost similar to the AA8110 alloy of AS. The development of the intermetallic compound and free micro-cracks in the SZ have provided a more effective joint.
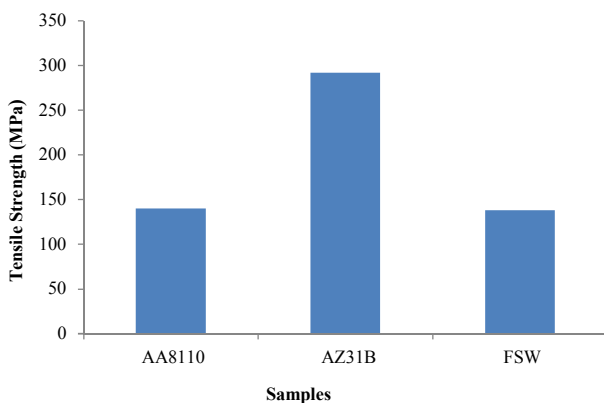

Fig. 15. Tensile Strength under optimal welding condition

6. CONCULSIONS

In this paper, the L16 orthogonal array is used to conduct an experiment on the welding of an AA8011–AZ31B dissimilar alloy. The welding parameters are optimized with the aid of ANN-GA to improve the performance of the joint. The findings of this investigation are concluded as below.

- The AA7475–AZ31B alloy is welded successfully by the FSW operations. The performance of the weld quality is measured through the mechanical characterization studies of microhardness and tensile strength.
- The influence of parameters on the hardness and tensile strength is investigated and it is noted that parameters such as tool type, welding speed and rotational speed have played a major role in the quality of welding.
- FSW process parameters such as tool type, rotational speed and welding speed are optimized using ANN-GA. The predicted optimizing parameter ranges are mentioned as the taper cylindrical pin tool, welding speed of 21 mm/min and rotational speed of 1182 rpm. The output responses, which are predicted through the ANN-GA, have provided the tensile strength of 138.46 MPa and hardness of 85.57 Hv.

REFERENCES

[1] R.K. Jayaraj, S. Malarvizhi, and V. Balasubramanian, "Electrochemical corrosion behaviour of stir zone of friction stir welded dissimilar joints of AA6061 aluminium–AZ31B magnesium alloys", *Trans. Nonferrous Met. Soc. China*, vol. 27, pp. 2181–2192, 2017.

[2] S. Eacherath and S. Murugesan, "Synthesis and characterization of magnesium-based hybrid composites – A review", *Int. J. Mater. Res.*, vol. 109, no. 7, pp. 661672, 2018.

[3] K.O. Cooke, A. Alhazaa, and A.M. Atieh, "Dissimilar Welding and Joining of Magnesium Alloys: Principles and Application", in *Magnesium – The Wonder Element for Engineering/Biomedical Applications*, M. Gupta, Ed., Intechopen, 2019, pp. 1–20.

[4] T. Sun, M.J. Roy, D. Strong, P.J. Withers, and P.B. Prangnell, "Comparison of residual stress distributions in conventional and stationary shoulder high-strength aluminum alloy friction stir welds", *J. Mater. Process. Technol.*, vol. 242, pp. 92–100, 2017.

[5] H. Lina, Y. Wua, and S. Liu, "Impact of initial temper of base metal on microstructure and mechanical properties of friction stir welded AA 7055 alloy", *Mater. Charact.*, vol. 146, pp. 159–168, 2018, doi: 10.1016/j.jmapro.2018.04.017.

[6] H.J. Aval and A. Loureiro, "Effect of reverse dual rotation process on properties of friction stir welding of AA7075 to AISI304", *Trans. Nonferrous Met. Soc. China*, vol. 29, pp. 964–975, 2019, doi: 10.1016/S1003-6326(19)65005-3.

[7] N.Z. Khan, A.N. Siddiquee, Z.A. Khan, and A.K. Mukhopadhyay, "Mechanical and microstructural behavior of friction stir welded similar and dissimilar sheets of AA2219 and AA7475 aluminum alloys", *J. Alloys Compd.*, vol. 695, pp. 2902–2908, 2017, doi: 1 0.1016/j.jallcom.2016.11.389.

[8] S. Jannet, P.K. Mathews, and R. Raja, "Comparative investigation of friction stir welding and fusionwelding of 6061 T6 – 5083 O aluminum alloy based on mechanical properties and microstructure", *Bull. Pol. Acad. Sci. Tech. Sci.*, vol. 62, no. 4, pp. 791–795, 2014.

[9] M.K. Kulekci, U. Esme, F. Kahraman, and S. Ocalir, "Advanced hybrid welding and manufacturing technologies", *Mater. Test.*, vol. 58, no. 4, pp. 362–370, 2016, doi: 10.3139/120.110858.

[10] B. Çevik, Y. Özçatalbaş, and B. Gülenç, "Effect of tool material on microstructure and mechanical properties in friction stir welding", *Mater. Test.*, vol. 58, no. 1, pp. 36–42, 2016, doi: 10.3139/120.110816.

[11] I. Kucukrendec, "The investigation of suitable welding parameters in poly propylene sheets joined with friction stir welding", *Bull. Pol. Acad. Sci. Tech. Sci.*, vol. 67, no. 1, pp. 133–140, 2019.

[12] I. Kucukrendec, "Mechanical and microstructural properties of EN AW-6060 aluminum alloy joints produced by friction stir welding", *Bull. Pol. Acad. Sci. Tech. Sci.*, vol. 63, no. 2, pp. 475–478, 2015.

[13] G. Kumar, R. Kumar, and R. Kumar, "Optimization of process parameters of friction stir welded AA5082-AA7075 butt joints using resonance fatigue properties", *Bull. Pol. Acad. Sci. Tech. Sci.*, vol. 68, no. 1, pp. 99–108, 2020.

[14] W. Guo, G. You, G. Yuan, and X. Zhang, "Microstructure and mechanical properties of dissimilar inertia friction welding of 7A04 aluminum alloy to AZ31 magnesium alloy", *J. Alloys Compd.*, 2017, vol. 695, pp. 3267–3277, doi: 10.1016/j.jallcom.2016.11.218.

[15] Z. Liu, S. Ji, and X. Meng, "Improving Joint Formation and Tensile Properties of Dissimilar Friction Stir Welding of Aluminum and Magnesium Alloys by Solving the Pin Adhesion Problem", *J. Mater. Eng. Perform.*, vol. 27, no. 3, pp. 1404–1413, 2018, doi: 10.1007/s11665-018-3216-y.

[16] M. Ravichandran, M. Thirunavukkarasu, S. Sathish, and V. Anandakrishnan, "Optimization of welding parameters to attain maximum strength in friction stir welded AA7075 joints", *Mater. Test.*, vol. 58, no. 3, pp. 206–210, 2016, doi: 10.3139/120.110838.

[17] N. Sabarirajan and A.N. Sait, "Optimization and thermal analysis of friction stir welding of AA 6061-AA 8011 joints", *Mater. Test.*, vol. 62, no. 3, pp. 317–328, 2020, doi: 10.3139/120.111473.

[18] S. Deshwal, A. Kumar, and D. Chhabra, "Exercising hybrid statistical tools GA-RSM, GA-ANN and GA-ANFIS to optimize FDM process parameters for tensile strength improvement", *CIRP J. Manuf. Sci. Technol.*, vol. 31, no. 4, pp. 189–199, 2020, doi: 10.1016/j.cirpj.2020.05.009.

[19] S.C. Cagan, M. Aci, B.B. Buldum, and C. Aci, "Artificial neural networks in mechanical surface enhancement technique for the prediction of surface roughness and microhardness of magnesium alloy", *Bull. Pol. Acad. Sci. Tech. Sci.*, vol. 67, no. 4, pp. 729–739, 2019.

[20] H.D. Naghibi, M. Shakeri, and M. Hosseinzadeh, "Neural Network and Genetic Algorithm Based Modeling and Optimization of Tensile Properties in FSW of AA 5052 to AISI 304 Dissimilar Joints", *Trans. Indian Inst. Met.*, vol. 69, pp. 891–900, 2016, doi: 10.1007/s12666-015-0572-2.

[21] Y. Rong *et al.*, "Parameters optimization of laser brazing in crimping butt using Taguchi and BPNN-GA", *Opt. Lasers Eng.*, vol. 67, pp. 94–104, 2015, doi: 10.1016/j.optlaseng.2014.10.009.

[22] K.K. Babu *et al.*, "Parameter optimization of friction stir welding of cryorolled AA2219 alloy using artificial neural network modelling with genetic algorithm", *The Int. J. Adv. Manuf. Technol.*, vol. 94, pp. 3117–3129, 2018, doi: 10.1007/s00170-017-0897-6.

[23] A.S.F. Britto, R.E. Raja, and M.C. Mabel, "Prediction and optimization of mechanical strength of diffusion bonds using integrated ANN-GA approach with process variables and metallographic characteristics", *J. Manuf. Processes*, vol. 32, pp. 828–838, 2018, doi: 10.1016/j.jmapro.2018.04.015.

[24] H. Wang, Z. Zhang, and L. Liu, "Prediction and fitting of weld morphology of Al alloy-CFRP welding-rivet hybrid bonding joint based on GA-BP neural network", *J. Manuf. Processes*, vol. 63, pp. 109–120, 2021, doi: 10.1016/j.jmapro.2020.04.010.

[25] S. Chen, H. Zhang, X. Jiang, T. Yuan, Y. Han, and X. Li, "Mechanical properties of electric assisted friction stir welded 2219 aluminum alloy," *J. Manuf. Processes*, vol. 44, pp. 197–206, 2019, doi: 10.1016/j.jmapro.2019.05.049.

[26] A. Kumar and L.S. Raju, "Influence of tool pin profiles on friction stir welding of copper", *Mater. Manuf. Processes*, vol. 27, no. 12, pp. 414–1418, 2012, doi: 10.1080/10426914.2012.689455.

[27] B. Cieniawska, K. Pentoś, and D. Łuczycka, "Neural modeling and optimization of the coverage of the sprayed surface", *Bull. Pol. Acad. Sci. Tech. Sci.*, vol. 68, no. 3, pp. 601–608, 2020.

[28] D. Rajeev, D. Dinakaran, and S.C.E. Singh, "Artificial neural network based tool wear estimation on dry hard turning processes of AISI4140 steel using coated carbide tool", *Bull. Pol. Acad. Sci. Tech. Sci.*, vol. 65, no. 4, pp. 553–559, 2017.

[29] Y. Li, B. Yub, B. Wang, T.H. Lee, and M. Banu, "Online quality inspection of ultrasonic composite welding by combining artificial intelligence technologies with welding process signatures", *Mater. Des.*, vol. 194, pp. 108912, 2020.

[30] P.Q. Baban and I.N. Rahimabadi, "Input-output pairing criterion applied in the genetic algorithm for unstable linear systems", *Bull. Pol. Acad. Sci. Tech. Sci.*, vol. 64, no. 4, pp. 873–876, 2016.

[31] A. Abdollahzadeh, A. Shokuhfar, J.M. Cabrera, A.P. Zhilyaev, and H. Omidvar, "In-situ nanocomposite in friction stir welding of 6061-T6 Aluminum alloy to AZ31 magnesium alloy", *J. Mater. Process. Technol.*, vol. 263, pp. 296–307, 2019, doi: 10.1016/j.jmatprotec.2018.08.025.

[32] A.H. Baghdadi, Z. Sajuri, N.F.M. Selamat, M.Z. Omar, Y. Miyashita, and A.H. Kokabi, "Effect of intermetallic compounds on the fracture behavior of dissimilar friction stir welding joints of Mg and Al alloys," *Int. J. Miner. Metall. Mater.*, vol. 26, no. 10, pp. 1285–1298, 2019.

[33] L. Zhanga and X. Wanga, "Microstructure Evolution and Properties of Friction Stir Welding Joint for 6082-T6 Aluminum Alloy", *Mater. Res.*, vol. 21, no. 6, pp. e20180285, 2018.

[34] C.L. Yang, C.S. Wu, and X.Q. Lv, "Numerical analysis of mass transfer and material mixing in friction stir welding of aluminum/magnesium alloy", *J. Manuf. Processes*, vol. 32, 380–394, 2018.

[35] V.P. Singh, S.K. Patel, A. Ranjan, and B. Kuriachen, "Recent research progress in solid state friction-stir welding of aluminium–magnesium alloys: a critical review", *J. Mater. Res. Technol.*, vol. 9, no. 3, pp. 6217–6256, 2020.

[36] W. Hu, Z. Ma, S. Ji, Q. Song, M. Chen, W. Jiang, "Improving the mechanical property of dissimilar Al/Mg hybrid friction stir welding joint by PIO-ANN", *J. Mater. Sci. Technol.*, vol. 53, pp. 41–52, 2020.

[37] Z. Liang, G. Qin, L. Wang, X. Meng, and F. Li, "Microstructural characterization and mechanical properties of dissimilar friction welding of 1060 aluminum to AZ31B magnesium alloy", *Mater. Sci. Eng., A*, vol. 645, pp. 170–180, 2015.

[38] J. Verma, R.V. Taiwade, C. Reddy, and R.K. Khatirkar, "Effect of Friction Stir Welding Process Parameters on Mg-AZ31B/Al-AA6061 Joints," *Mater. Manuf. Processes*, vol. 33, no. 3, pp. 1–26, 2017.

Bull. Pol. Acad. Sci. Tech. Sci., vol. 70, no. 1, p. e140098, 2022

7